



Effect of Zinc Acetate Concentration on Structural, Optical and Electrical Properties of ZnO Thin Films Deposited by Electrostatic Spray on an ITO Substrate

Bhavana N. Joshi,^a Hyun Yoon,^a Ho Young Kim,^a Joon Ho Oh,^b Tae Yeon Seong,^{b,*} Scott C. James,^c and Sam S. Yoon^{a,z}

^aSchool of Mechanical Engineering, Korea University, Anamdong, Seongbukgu, Seoul 136-713, Korea

^bSchool of Materials Science and Engineering, Korea University, Anamdong, Seongbukgu, Seoul 136-713, Korea

^cThermal/Fluid Science & Engineering, Sandia National Laboratories, Livermore, California 94551, USA

Polycrystalline zinc oxide (ZnO) thin films were fabricated on indium tin oxide (ITO) substrates by electrostatic spray deposition using propylene glycol as the solvent for potential use in bulk heterojunction polymer solar cells. The microstructure and characteristics of the ZnO/ITO bilayer have been investigated for various precursor concentrations using SEM, AFM, X-ray diffraction, and UV-Visible spectroscopy. The bandgap energy of the bilayer slightly decreases when the zinc acetate dihydrate concentration in the propylene glycol solvent increases from 0.1 to 0.3 M. The ZnO/ITO bilayer shows high figure of merit ($12.4 \times 10^{-3} \Omega^{-1}$) and low resistivity ($3.78 \times 10^{-3} \Omega\text{-cm}$) for a Zn precursor concentration of 0.2 M.

© 2012 The Electrochemical Society. [DOI: 10.1149/2.077208jes] All rights reserved.

Manuscript submitted May 2, 2012; revised manuscript received June 4, 2012. Published July 20, 2012.

Zinc oxide (ZnO) thin films form transparent conducting oxides because of their appropriate electro-optical properties such as a wide bandgap (3.25 eV),¹ large exciton-binding energy (60 meV) yielding effective excitonic UV emissions, and high optical gain (300 cm^{-1})² at room temperature. In addition, ZnO is inexpensive and non-toxic, which makes it attractive for many industrial applications³ such as energy-efficient windows, liquid crystal displays, optoelectronic devices, ultrasonic oscillators, transducers, solar cells (a-Si, CIGS, inorganic thin film, and flexible polymer), gas sensors,⁴ UV luminescence devices, light emitting diodes,⁵ integrated optics, antireflection coatings, lasers diodes, UV range detectors, photodegradation, photocatalysis, superhydrophobic or self-cleaning surfaces,² and transistors.⁶

ZnO thin films have been produced with various vacuum-based techniques, such as RF magnetron sputtering,⁷ metal organic chemical vapor deposition,⁸ plasma-assisted molecular beam epitaxy,⁹ and pulsed laser deposition.¹⁰ However, these techniques require expensive vacuum chambers yielding restrictive operating conditions (e.g., limited coating area); thus alternative techniques are needed. In general, sol-gel,¹¹ spray pyrolysis,⁶ dip coating,¹² and electrostatic spray deposition (ESD)¹³ are considered cost-effective alternative deposition methods. Among these, spray-based methods are preferred for coating large areas and ESD is particularly attractive because it produces extremely fine (sub-micron), self-dispersive (non-agglomerating), highly wettable (electrowetting) adhesive droplets that yield a uniform coating on the substrate; see Fig. 1a. In addition, because charged droplets are accelerated toward the substrate, ESD offers improved targeting, which results in high deposition efficiency and low material consumption.¹⁴ Using the ESD aerosol technique, organic solvents containing inorganic or organometallic precursors can be dispersed into micrometer-sized, charge carrying droplets under an imposed electric field.¹⁵

The precursor, containing dissolved salts (zinc acetate dihydrate in this case), is pumped through a metal nozzle, and high voltage (typically 6 to 15 kV) is applied between the nozzle (anode) and the grounded substrate (cathode). The fluid emerging from the tip of the nozzle (precursor) assumes a conical shape (Taylor cone) due to the applied voltage and ultimately yields a spray of positively charged droplets.¹⁶ The self-dispersed droplets are attracted to the grounded substrate, which is heated to induce thermal pyrolysis. After droplet impingement onto the substrate, the charges migrate to ground and the solvent evaporates leaving only the desired inorganic or organometallic product, which forms the thin film.

Ghimbeu et al.¹⁷ produced ZnO thin films on a platinum-coated alumina substrate with ESD using a mixture of zinc acetate dihydrate,

ethanol, and hydrochloric acid as a precursor; these films have gas sensing applications. Hwang et al.¹⁸ deposited transparent ZnO thin films having a bandgap range of 3.24 to 3.28 eV onto a soda-lime-silica glass using zinc acetate, 2-methoxy ethanol, and 2-aminoethanol as the mixture. Zinc-nitrate with water and iso-propanol were used as the mixture by Zaouk et al.⁴ to deposit *c*-axis-oriented thin films on a tin oxide-deposited Corning 7059 glass substrate at 350°C for piezoelectric thin-film applications. Polycrystalline ZnO thin films were deposited on a silicon wafer by Li et al.⁵ from hydrothermally synthesized ZnO nanocrystals using a zinc acetate ethanol precursor for UV luminescence devices.

An efficient and uniform coating is obtained when the tip of the electrostatic spray nozzle issues a stable cone jet. Stability generally depends on the surface tension, electrical conductivity, and viscosity of the working solvent. In the present study, propylene glycol (PG) is used as the solvent due to its high surface tension (40.1 mN/m) and viscosity (56 mPa-s) compared to that of the more commonly used ethanol with a surface tension of 22.4 mN/m and viscosity of 1.2 mPa-s. A stable cone-jet is easily obtained using PG as a solvent. An ITO substrate is used for potential application in bulk heterojunction polymer solar cells, which typically use ZnO as the *n*-type metal oxide because of its relatively high electron mobility and high transparency. Also, ZnO can be used as an electrode layer for CIS-based solar cells. Furthermore, using ITO as a seed layer for the ZnO films yields a high quality transparent conducting oxide because of a small lattice mismatch between the (111) plane of ITO and the (001) plane of ZnO.^{19,20} Although there have been other studies on ESD fabrication of ZnO films, to the best of our knowledge, the effects of precursor concentration on the microstructure and characteristics of these ZnO films are not available. While varying zinc acetate dihydrate precursor concentrations, we characterize the resulting thin films using SEM, AFM, X-ray diffraction, UV-Vis spectroscopy and Hall effect measurements.

Experimental

Zinc acetate dihydrate of concentrations of 0.1–0.3 M were dissolved in PG (99.9% purity) and used as the precursor solutions to make ESD ZnO thin films. Often, ZnO is doped with Al to achieve low resistivity in the range of $\sim 10^{-4} \Omega\text{-cm}$. In these experiments, however, the ZnO precursor was not doped so film resistivity was in the range of $\sim 10^{-3} \Omega\text{-cm}$. The ESD setup is depicted in Fig. 1b. The ITO coated glass used as conductive substrate was purchased from market. The precursor solution was pumped through a 4-mm-diameter metal nozzle at a flow rate of 75 $\mu\text{L}/\text{hour}$. The conductive ITO coated glass substrate ($2 \times 1 \text{ cm}^2$) was maintained at 200°C to facilitate the rapid drying of the precursor (boiling temperature of PG is 188°C). The

*Electrochemical Society Active Member.

^zE-mail: skyoon@korea.ac.kr

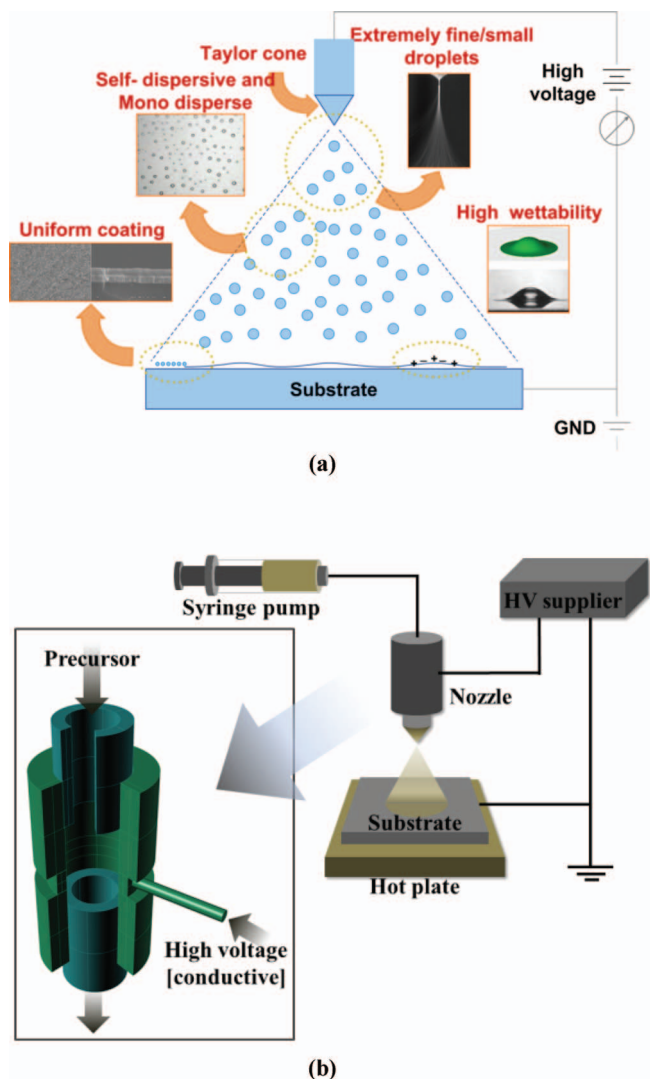


Figure 1. (a) Advantages of the ESD thin film coating technique. (b) Schematic of the ESD setup.

spray duration was 30 min and the distance between the nozzle and substrate was 30 mm. A voltage of 11.25 kV was applied to the nozzle to form the Taylor cone that develops a few 10^2 nm-size droplets. The semi-vertical angle of Taylor cone is observed to be 43.3° which is less than the angle reported by Taylor (49.3°). Such low Taylor cone angle have been previously reported.^{21,22} Following deposition, the film was annealed at 500°C in a closed chamber oven at 1 atm for one hour to remove organic contamination from the precursor solution and also to improve the crystallinity and adhesion of the film. Before deposition, the various-concentration precursor solutions were characterized using a Brookfield Viscometer, surface tension analyzer, and conductivity meter to determine their viscosities, surface tensions, and conductivities, respectively. The structures of the films were characterized with X-ray diffraction measurements (XRD, Rigaku Japan, D/max-2500) using CuK α (radiation $k = 0.154$ nm). The surface morphologies of the films were investigated using a scanning electron microscope (HRSEM, Philips, XL30SFEG at 10 kV). Cross sections were visualized using the SEM to estimate film thicknesses. A non-contact mode atomic force microscope (AFM Park Systems Xe-100) was used to examine the surface morphology and roughness of the electro-sprayed films. Film transmission was measured with a double beam UV-visible spectrometer (4974 SPEC-Unicam UV-530). Electrical properties were measured using a Hall device (Ecopia HMS-3000) with the Van der Pauw method. The electrical proper-

Table I. Properties of precursor solutions; density (ρ), surface tension (γ), conductivity (κ) and viscosity (η).

Solvent/Precursors [M]	ρ [g/cc]	γ [mN/m]	κ [$\mu\text{S}/\text{cm}$]	η [mPa · s]
PG	1.04	40.1	0.1	56.0
0.1	1.06	34.0	17.9	40.3
0.2	1.10	33.8	27.0	38.7
0.3	1.10	31.5	34.4	36.9

ties of the films reported herein are the mean values from at least three repeatable tests.

Results and Discussion

Precursor properties are presented in Table I. Compared to the properties of pure PG, the viscosity and surface tension of the precursor solution decrease with increasing zinc acetate dihydrate concentration. The electrical conductivities of the precursors (not the films) increase with increased zinc acetate dihydrate concentration. Note that the electrical conductivity affects the flowrate of the precursors.¹⁴

The crystal structure and orientation of the ZnO/ITO thin films deposited at various zinc acetate dihydrate precursor concentrations were examined by X-ray diffraction (XRD) operating in a Bragg-Brentano configuration with a 2θ range of 20 to 70° . The XRD patterns are shown in Fig. 2. The pronounced diffraction peaks indicate that the films are polycrystalline and that the peaks are consistent with the diffraction planes of the hexagonal wurtzite structure mentioned in JCPDS data card no. 36-1451.²³ The peaks observed at diffraction angles of 31.4 , 34.4 , 36.1 , 56.1 , and 62.7° correspond to the (100), (002), (101), (110), and (103) planes of ZnO, respectively. The diffraction peaks corresponding to the ITO substrate are identified in Fig. 2 by black circles. The intensities of the ZnO peaks enhanced due to increase in thickness of films at higher zinc acetate dihydrate concentrations. The interplanar distance, d , and diffraction angle values are in agreement with the expected values.

Quantitative information about preferential crystal orientation can be collected from the texture coefficient (TC). The TC (hkl)²⁴ was calculated from X-ray data using the measured relative intensity of the (hkl) plane, and the standard intensity of a similar (hkl) plane²³ for the three diffraction peaks corresponding to (100), (002), and (101) planes. Fig. 3 shows variations of TC (hkl) for the peaks

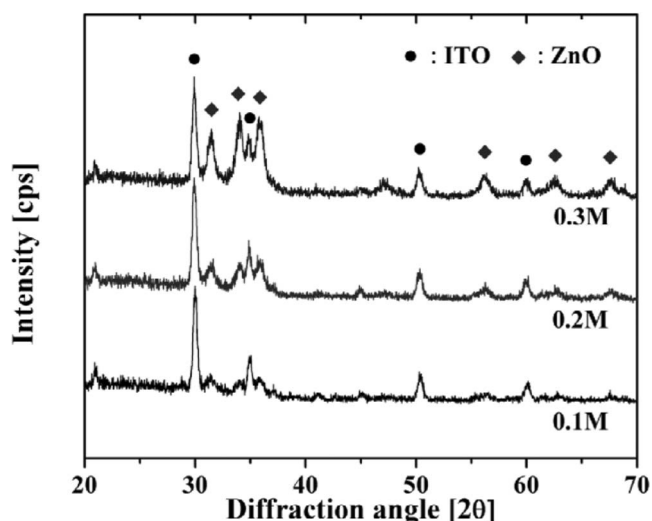


Figure 2. XRD patterns of ZnO thin film deposited on an ITO substrate at 0.1, 0.2, and 0.3 M zinc acetate dihydrate concentrations.

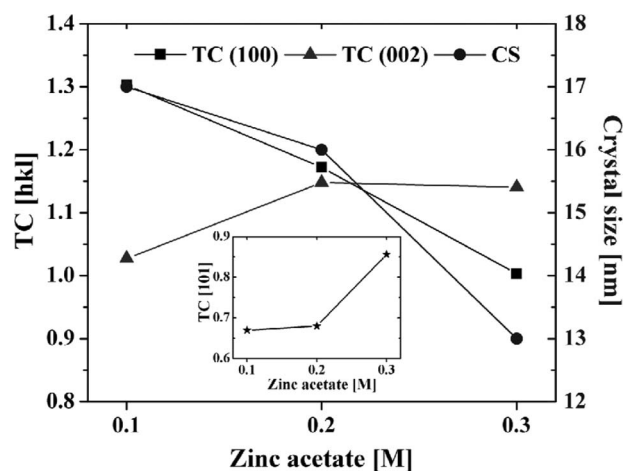


Figure 3. Variation of the texture coefficient, TC (hkl), and crystal size with zinc acetate dihydrate concentration.

corresponding to planes (100), (002), and (101) (shown in inset). It is observed that the TC for the (101) plane increases and the TC for the (100) plane decreases with increasing zinc acetate dihydrate concentration. The TC for the (002) plane is highest at 0.2 M, which implies that most of the precursor solution decomposed completely and formed grains along the (002) plane. It is observed that the increase in zinc acetate concentration gives rise to *c*-axis (002) oriented thin films. The average crystal size of these grains was measured using the Debye-Scherrer formula²⁵ assuming a shape factor of 0.95. As shown in Fig. 3, the average crystal size of ZnO demonstrates nanocrystallinity (<100 nm) and crystal size decreases with increasing zinc acetate dihydrate concentration. This is due to decrease in droplet size in electrostatic spray; Yoon et al.¹⁴ demonstrated that increased conductivity decreased droplet size. The lattice parameters *a* for the (100) plane and *c* for the (002) plane² were determined using their respective diffraction angles θ . The estimated lattice parameters are in agreement with the values noted on the JCPDS data card.

The *d* values of the (002) and (101) planes are larger than those from JCPDS data; this means that the 2θ values are shifted downward for the 0.1 M concentration, but the 2θ values increase with increasing zinc acetate dihydrate concentration. This lateral shift of the diffraction peak is due to the stress generated in the thin films by defects in the lattice. Stress (σ)²⁶ in the ZnO thin films are estimated using a bulk lattice constant of *c* = 0.5206 nm. The values of the lattice constants *a*, *c*, and σ are presented in Table II. Negative values of σ represent compressive stresses in the films due to porosity and oxygen deficiencies. Decreased compressive stresses for the 0.3 M zinc acetate dihydrate concentration films are due to reduced porosity

Table II. Lattice constants (*a*, *c*) and stress (σ) from XRD data.

	0.1 M	0.2 M	0.3 M	JCPDS Values
<i>a</i> [nm]	0.3284	0.3282	0.3282	0.3249 nm
<i>c</i> [nm]	0.5270	0.5273	0.5252	0.5206 nm
σ [GPa]	-5.563	-5.587	-4.009	Stress free

and improved crystallinity, which are also confirmed by the reduced average roughness values of the AFM data.

The surface morphology of the films was examined by SEM. Micrographs of the ZnO films resulting from different zinc acetate dihydrate concentrations are depicted in the top row of Fig. 4. The films have a porous morphology similar to the morphology observed by Wang et al.,²⁷ who deposited Fe₂O₃ by ESD using PG as a solvent. In our study, the porosity decreased with increasing zinc acetate dihydrate concentration. Cross-sectional views of the films are shown on the bottom row of Fig. 4; the thicknesses of the films increase from 442 to 950 nm with increasing zinc acetate dihydrate concentration, which is in agreement with the XRD data shown in Fig. 2.

The elemental composition of the ZnO film deposited at a substrate temperature of 200°C and annealed for 1 hr at 500°C was measured by EDAX analysis. Fig. 5 shows the EDAX spectrum of a 0.1 M film; the characteristic peaks of Zn and O are evident. Theoretically expected stoichiometric mass percent of zinc and oxygen in ZnO are 80.3 and 19.7% respectively.²⁸ The mass percentage of zinc and oxygen is observed to be 80.60 and 19.40 for 0.1 M concentration of Zinc precursor. The peaks at 1.7 and 2.1 keV indicate the silicon present in the glass substrate and the platinum coating that was deposited on the film to prevent charge buildup. Peaks corresponding to indium and tin from the substrate are also observed, as well as other peaks that indicate the elemental components of the sample holder.

The two- and three-dimensional images presented in Fig. 6 show the surface roughness of the ZnO films, as measured by AFM. Both SEM and AFM images indicate that a highly uniform film was produced by the ESD technique with surface roughness less than 12 nm. These images qualitatively demonstrate that the higher the zinc acetate dihydrate concentration, the smoother the film surface. Average roughness values determined from the XEI data processing analysis software available with the AFM system are 11.82, 8.55 and 7.89 nm for the films produced with 0.1, 0.2, and 0.3 M concentrations, respectively; the average surface roughness of the ITO substrate was 0.5 nm. ZnO films have decreased surface roughness with increased zinc acetate dihydrate concentration due to densification of the film. The roughness values are high, 11.82 nm, for the 0.1 M zinc acetate dihydrate precursor because of the film's higher porosity, but the films become thicker and denser with increased zinc acetate dihydrate concentration. With increased zinc acetate dihydrate concentration, the

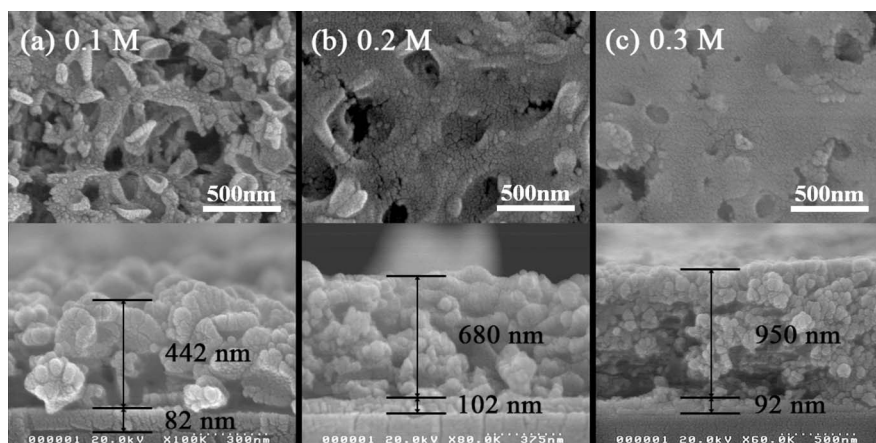


Figure 4. SEM images showing surface (top) and cross sectional (bottom) views of films. The thickness of the ITO substrate range from 88 to 102 nm.

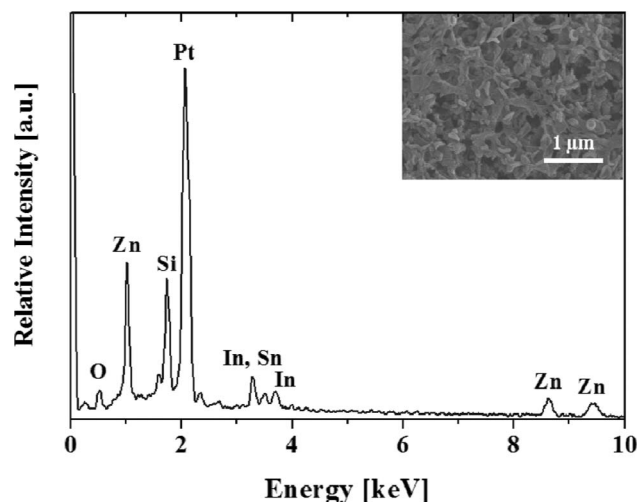


Figure 5. EDAX spectrum of the 0.1 M ZnO film deposited on ITO and annealed at 500°C.

droplets reaching the substrate contain more salt and less solvent, which means less evaporation of the solvent, and as a result, a less porous or more compact film is formed. Less porous films with increased dissolved salt concentrations were also observed by Hossain

et al.²⁹ who carried out dip coating using ethanol as the solvent. Besides the precursor concentration, densification or porosity control of the films are also related to other factors, such as droplet size, precursor's thermo-physical properties, substrate temperature, and solvent boiling point, all of which impact the evaporation process of the solvent.

Table I indicates that the electrical conductivity of the precursors increases when the Zn concentration increases, which in turn decreases the droplet size according to Yoon et al.¹⁴ and Matsushima et al.³⁰ Reasonably small droplets facilitate efficient solvent evaporation, contributing to the formation of denser films. It is noteworthy that the substrate temperature also influences the surface morphology of the film because it affects the solvent evaporation rate. For example, if the droplets have mostly evaporated prior to their impact (either due to high substrate temperature or too small of a droplet size), the film becomes porous upon dried particle accumulation. If the droplets were excessively large or the substrate temperature was too low, then ESD would yield similar results as sol-gel or dip coating and the advantages of spray deposition would be lost. Also, in general, solvents with high boiling points are preferred if a dense film is to be fabricated. The higher the boiling point, the slower the evaporation, and thus slower the precipitation of the salts in the precursor and higher the film density.³¹

Fig. 7 shows the wavelength dependence of the optical transmittance spectra for ZnO/ITO thin films. Of course, the transmittance of film plus substrate is less than that of the substrate alone. As the zinc acetate dihydrate concentration increases, the film becomes denser

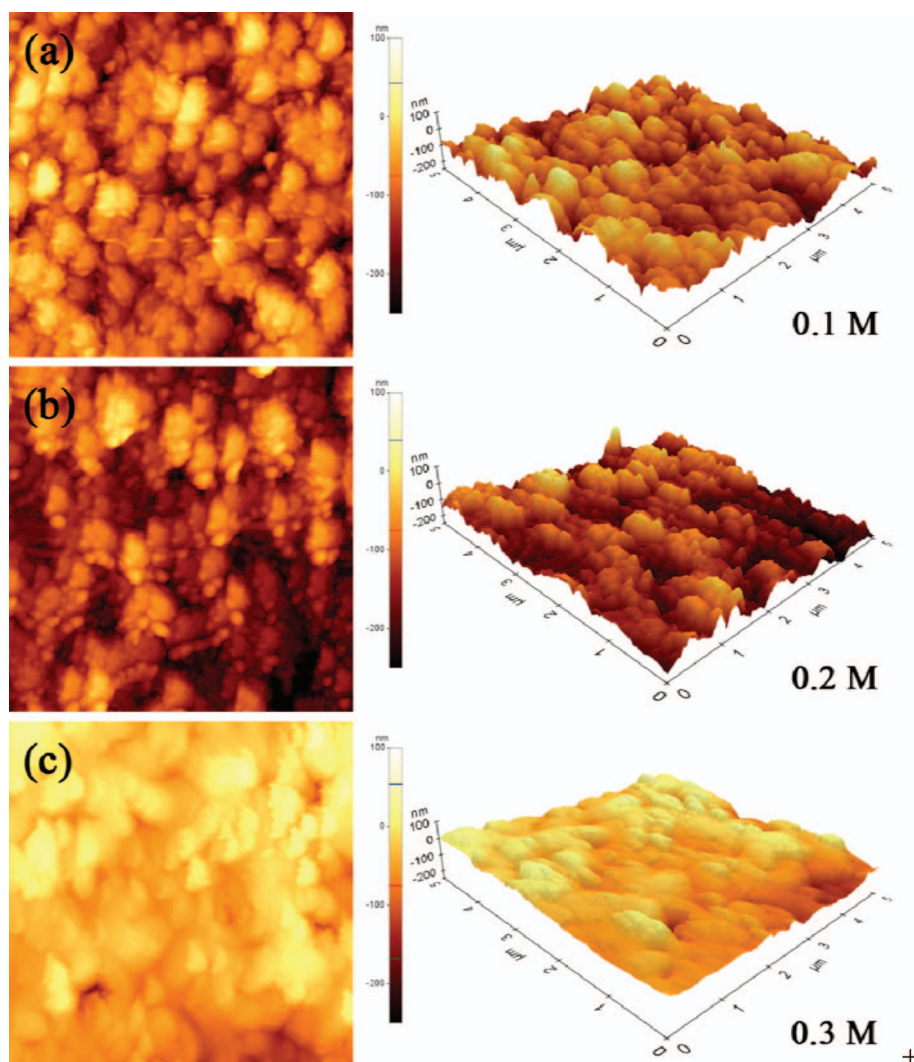


Figure 6. AFM images showing surface morphologies of ZnO films for zinc acetate dihydrate concentrations of (a) 0.1 M, (b) 0.2 M, and (c) 0.3 M.

Table III. Electrical properties.

Samples	ρ [$\times 10^{-3} \Omega\text{-cm}$]	κ [S/cm]	μ [$\text{cm}^2/\text{V}\cdot\text{s}$]	n_e [$\times 10^{19} \text{cm}^{-3}$]	FOM [$\times 10^{-3} \Omega^{-1}$]	t [nm]
ITO	0.21	4694	48.2	-60.74	-	100
0.1 M	3.49	287	54.9	-3.26	9.1	524
0.2M	3.78	268	55.9	-2.95	12.4	782
0.3M	5.40	185	54.1	-2.14	7.9	1042

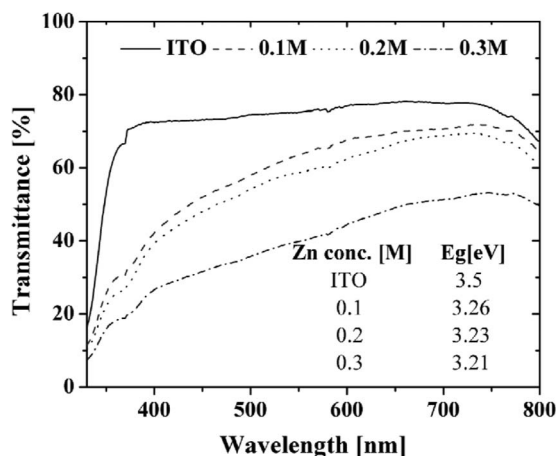


Figure 7. Transmittance spectra of the ITO substrate and ZnO thin films for various zinc acetate dihydrate concentrations in the precursor.

and thicker, decreasing the transmittance of the film. The transmittance of the film can also be decreased by light scattering in the film; however the fact that the film density increases with increasing zinc acetate dihydrate concentration with minimal change in film roughness suggests that scattering does not play a significant role. The absorption coefficient, α , which corresponds to electron excitation from the valance band to the conduction band, is used to determine the optical bandgap energy using Lambert's formula,¹² $\alpha = (1/t) \log(1/T)$, where t is thickness and T is film transmittance. The optical bandgap energies

of the ITO substrate and ZnO films are determined by extrapolating the linear portion of the $(\alpha h\nu)^2$ vs. $h\nu$ plot. The bandgap value of the ITO substrate is estimated to be 3.5 eV and the bandgap energy of the ZnO films was found to be in the range from 3.26 to 3.21 eV (see the inset text of Fig. 7). These bandgap values are in good agreement with previously reported values of 3.14–3.26 eV^{3,18} for ZnO. Analyzing the bandgap data in more detail would suggest that the bandgap decreases with increasing zinc acetate dihydrate concentration. This decrease could be due to stress relaxation in the film. As shown in Table II, the stress in the film is compressive and it decreases with increasing zinc acetate dihydrate concentration. This decrease is attributed to film densification and an increase in oxygen content, which relaxes stresses in the film and also lowers the bandgap energy. The dependence of the bandgap on stress, through a change in oxygen content, was also reported by Mohanty et al.³² for aluminum-doped ZnO films. Lowering the film stress by increasing the concentration causes a reduction in the film's conductivity,³³ a slight reduction in the film's bandgap, and an increase in the film's resistivity.

The snapshots of water contact angles on the ITO substrate and ZnO film from 0.1 M concentration are shown in Fig. 8a and 8b, respectively. The ZnO film is significantly more hydrophilic (6.4°) than the ITO (67°) substrate, which is desirable for self-cleaning applications.

Electrical properties such as, resistivity (ρ), conductivity (κ), mobility (μ), and carrier concentration (n_e) of ZnO/ITO bilayer were measured using a Hall set up with the Van der Pauw method and results are presented in Table III. For these measurements, indium contacts were applied to the four corners of the ZnO thin films and the thicknesses of the ITO and thin films were properly taken into account. The current-voltage (I-V) curves for the films are linear, showing that the electrical properties of the films are Ohmic. As shown in Table III, ρ increases with film thickness, t . Khan et al.³⁴ observed that for SnO₂ films, as the films became smoother with increasing thickness, additional defects and strain variations, which can hinder the flow of electrons and increase resistivity occurred. Similarly, for ZnO thin films, as the film thickened, resistivity increased. The electron mobility was highest for 0.2 M precursor concentration due to the improvement in crystallinity whereas the carrier concentration n_e decreased with the increase in thickness. Figure of merit (FOM), which is the ratio of transmittance ($\lambda = 550 \text{ nm}$) to sheet resistance, is the parameter used to evaluate transparent conducting oxides. FOM values of ZnO/ITO bilayer is presented in Table III. The highest FOM value was $12.4 \times 10^{-3} \Omega^{-1}$ for the 0.2 M zinc acetate dihydrate concentration films.

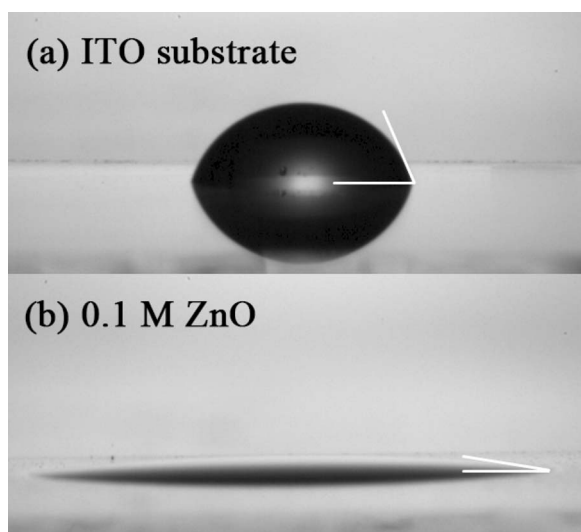


Figure 8. Water contact angle on (a) the ITO substrate (67°) and (b) the 0.1 M ZnO film (6.4°). This annealed film has a thickness of 442 nm, an average transmittance of 62% in the 400 to 800 nm wavelength range, and an average roughness of 11.82 nm.

Conclusions

The ESD technique was used to deposit a precursor comprising propylene glycol and zinc acetate dihydrate at various concentrations. The films were annealed at 500°C in a closed oven for one hour to remove organic contamination from the precursor solution and also to improve crystallinity and adhesion. AFM images showed high film roughness values for the 0.1 M zinc acetate dihydrate precursor; it also had the highest porosity. The bandgap energies of the thin films decreased from 3.26 to 3.21 eV when the precursor concentration increased from 0.1 to 0.3 M. The ZnO/ITO bilayer shows a high FOM ($12.4 \times 10^{-3} \Omega^{-1}$) and low resistivity ($3.78 \times 10^{-3} \Omega\text{-cm}$) for Zn precursor concentration of 0.2 M. These electro-sprayed ZnO films

can be applied to bulk heterojunction polymers and CIS-based solar cells, which typically use ZnO as the *n*-type metal oxide. Also, ESD-produced ZnO thin films showed superior hydrophilicity (low contact angle), which is advantageous for applications such as photocatalytic self-cleaning surfaces.

Acknowledgment

This work was supported by the Human Resources Development of the Korea Institute of Energy Technology Evaluation and Planning (KETEP, No. 20104010100640), National Research Foundation of Korea (NRF-2012-0001169), and the Converging Research Center Program through the Ministry of Education, Science and Technology (2010K000969). This work was also supported by the National Research Foundation of Korea (NRF-2011-0030433 and 2010-0010217) grant funded by the Korean government (MEST) and by a grant from the cooperative R&D Program (B551179-08-03-00) funded by the Korea Research Council Industrial Science and Technology. The first author acknowledges the support from the 2011 Postdoctoral Fellowship Program for Foreign Researchers.

References

1. D. Zhang, H. Yabe, E. Akita, P. Wang, R. Murakami, and X. Song, *J. Appl. Phys.*, **109**, 104318 (2011).
2. O. Lupan, T. Pauporté, L. Chow, B. Viana, F. Pellé, L. Ono, B. Roldan Cuenya, and H. Heinrich, *Appl. Surf. Sci.*, **256**, 1895 (2010).
3. B. Joseph, K. Gopchandran, P. Manoj, P. Koshy, and V. Vaidyan, *Bull. Mater. Sci.*, **22**, 921 (1999).
4. D. Zaouk, Y. Zaatari, R. Asmar, and J. Jabbour, *Microelectron. J.*, **37**, 1276 (2006).
5. J. Li, H. Fan, X. Jia, J. Chen, Z. Cao, and X. Chen, *J. Alloys Compd.*, **481**, 735 (2009).
6. G. Adamopoulos, A. Bashir, W. P. Gillin, S. Georgakopoulos, M. Shkunov, M. A. Baklar, N. Stingelin, D. D. C. Bradley, and T. D. Anthopoulos, *Adv. Funct. Mater.*, **21**, 525 (2011).
7. Y. Jouane, S. Colis, G. Schmerber, C. Leuvrey, A. Diniá, P. Leveque, T. Heiser, and Y.-A. Chapuis, *J. Mater. Chem.*, **22**, 1606 (2012).
8. A. Hongsingthong, I. Afdi Yunaz, S. Miyajima, and M. Konagai, *Sol. Energy Mater. Sol. Cells*, **95**, 171 (2011).
9. P. Ding, X. Pan, J. Huang, H. He, B. Lu, H. Zhang, and Z. Ye, *J. Cryst. Growth*, **331**, 15 (2011).
10. M. Lorenz, G. Wagner, A. Rahm, H. Schmidt, H. Hochmuth, H. Schmid, W. Mader, M. Brandt, H. von Wenckstern, and M. Grundmann, *Phys. Status Solidi C*, **5**, 3280 (2008).
11. Y. Sun, J. H. Seo, C. J. Takacs, J. Seifert, and A. J. Heeger, *Adv. Mater.*, **23**, 1679 (2011).
12. T. Ratana, P. Amornpitoksuk, and S. Suwanboon, *J. Alloys Compd.*, **470**, 408 (2009).
13. A. Hosseinmardi, N. Shojaei, M. Keyanpour-Rad, and T. Ebadzadeh, *Ceram. Int.*, **38**, 1975 (2012).
14. H. Yoon, J. H. Woo, Y. M. Ra, S. S. Yoon, H. Y. Kim, S. J. Ahn, J. H. Yun, J. Gwak, K. H. Yoon, and S. C. James, *Aerosol Sci. Technol.*, **45**, 1448 (2011).
15. A. Jaworek, *J. Mater. Sci.*, **42**, 266 (2007).
16. M. Cloupeau and B. Prunet-Foch, *J. Electrostatics*, **22**, 135 (1989).
17. C. M. Ghimbeu, J. Schoonman, M. Lumberras, and M. Siadat, *Appl. Surf. Sci.*, **253**, 7483 (2007).
18. K. S. Hwang, J. H. Jeong, Y. S. Jeon, K. O. Jeon, and B. H. Kim, *Ceram. Int.*, **33**, 505 (2007).
19. X. Teng, H. Fan, S. Pan, C. Ye, and G. Li, *J. Phys. D: Appl. Phys.*, **39**, 471 (2006).
20. X. Chen, X. Geng, J. Xue, and L. Li, *J. Cryst. Growth*, **299**, 77 (2007).
21. A. Yarin, S. Koombhongse, and D. Reneker, *J. Appl. Phys.*, **90**, 4836 (2001).
22. S. Reznik, A. Yarin, A. Theron, and E. Zussman, *J. Fluid Mech.*, **516**, 349 (2004).
23. P. D. File, *Joint Committee on Powder Diffraction Standards, Swarthmore, PA*, Card No. 36 (2000).
24. S. Ilican, Y. Caglar, M. Caglar, and B. Demirci, *J. Optoelectron. Adv. Mater.*, **10**, 2592 (2008).
25. L. Ghule, A. Patil, K. Sapnar, S. Dhole, and K. Garadkar, *Toxicol. Environ. Chem.*, **93**, 623 (2011).
26. S. Maniv, W. Westwood, and E. Colombini, *J. Vac. Sci. Technol.*, **20**, 162 (1982).
27. L. Wang, H. Xu, P. Chen, D. Zhang, C. Ding, and C. Chen, *J. Power Sources*, **193**, 846 (2009).
28. A. Bari, M. Shinde, V. Deo, and L. Patil, *Indian J. Pure Appl. Phys.*, **47**, 24 (2009).
29. M. Hossain, S. Biswas, M. Shahjahan, and T. Takahashi, *J. Vac. Sci. Technol., A*, **27**, 1047 (2009).
30. Y. Matsushima, Y. Nemoto, T. Yamazaki, K. Maeda, and T. Suzuki, *Sensors Actuators B: Chem.*, **96**, 133 (2003).
31. H. Yoon, J. H. Woo, B. Joshi, Y. M. Ra, S. S. Yoon, H. Y. Kim, S. J. Ahn, J. H. Yun, J. Gwak, and K. H. Yoon, *J. Electrochem. Soc.*, **159**, H444 (2012).
32. B. C. Mohanty, Y. H. Jo, D. H. Yeon, I. J. Choi, and Y. S. Cho, *Appl. Phys. Lett.*, **95**, 062103 (2009).
33. R. Menon, K. Sreenivas, and V. Gupta, *J. Appl. Phys.*, **103**, 094903 (2008).
34. A. F. Khan, M. Mehmood, A. Rana, and M. Bhatti, *Appl. Surf. Sci.*, **255**, 8562 (2009).